RESEARCH PAPER

Physicochemical and antimicrobial properties of post-synthesis betanin and chitosan oligosaccharide functionalized silver nanoparticles

K. M. Mbae · S. Umesha

Abstract Size uniformity and defined surface coating are important parameters for the biological properties of silver nanoparticles (AgNPs). Green synthesis uses biomolecules either in pure form or plant extracts as both reductants and stabilizers yielding a wide size range and capping composed of oxidation products and biomolecules present in the reaction mixture. Herein, we used an established methodology, silver nitrate as the metal precursor, and sodium citrate and tannic acid for reduction and stabilization to produce weakly passivated citrate capped AgNPs (CtAgNPs). Inductively coupled plasma mass spectrometry was used to determine the total concentration of silver in the purified nanoparticles colloidal dispersion and results correlated with absorbance at localized surface plasmon resonance (LSPR) peak for quick estimation of silver concentration. The CtAgNPs were functionalized with chitosan oligosaccharide (mean M_n 5000) and betanin to yield chitosan and betanin capped AgNPs. Their biocidal properties were tested against *Staphylococcus aureus* American Type Culture Collection (ATCC) 12,600. Citrate-stabilized AgNPs had a LSPR peak at 432 nm, mean core diameter of 37.9 ± 8.6 nm, and a monomodal distribution, and were roughly spherical. A slight red shift in LSPR peak was observed upon capping change. The minimum inhibitory concentration against *S. aureus* was 12.5 ppm Ag for all the nanoparticles. Our study advances the path of exploiting size reproducible techniques in AgNP synthesis, post-synthesis biomolecule functionalization for defined surface, and a clear procedure for estimating the concentration of Ag in assays. This is envisaged to encourage investigations with distinct sizes and capping for cross-comparison.

Keywords Silver nanoparticles · Chitosan oligosaccharide · Betanin · Post-synthesis functionalization · *Staphylococcus aureus*

Introduction

The distinctive properties of silver nanoparticles (AgNPs) are of interest to scientists in diverse areas of physical, chemical, and life sciences. They display the strongest surface plasmonic properties amongst coinage metal nanoparticles (Stamplecoskie 2015). This has endeared them to various applications in the areas of energy, catalysis, sensing, and biotherapy (Tran et al. 2013). Conversely, the exploitation of silver for its antimicrobial properties can be traced to the use of silver vessels for food preservation and the production of safe drinking water by early civilizations (Chernousova and Epple 2013). Upon discovery of its antibacterial properties, silver was introduced into the medical field for use in wound healing and burn treatment (Barillo and

K. M. Mbae · S. Umesha (✉)
Department of Studies in Biotechnology, University of Mysore, Manasagangotri, Mysuru, Karnataka 570006, India
e-mail: pmumesh@gmail.com
e-mail: su@appbot.uni-mysore.ac.in

K. M. Mbae
Department of Food Science, Meru University of Science and Technology, P.O.BOX 972, Meru 60200, Kenya

Marx 2014). The advent of antibiotics in the early 1940s led to the replacement of silver, predominantly by penicillin. Owing to appearance and an increase in antibiotic-resistant bacterial strains, silver has re-emerged as a promising material in the development of new bactericides (Chopra 2007). AgNPs have been incorporated into numerous personal care items and medications. These range from soaps, lotions, sanitizers, clothing, food packing containers, and food supplements (Tulve et al. 2015).

Many attributes of AgNPs are associated with their size and surface properties (Lee and El-Sayed 2006). Compared to their macroscale elemental form, AgNPs are thermodynamically unstable (Mcmahon et al. 2005; Phan and Haes 2019). This necessitates some form of surface stabilization. AgNPs are susceptible to surface oxidation and dissolution, releasing silver ions (Ag^+), which are largely accredited to their antimicrobial properties (Desireddy et al. 2013). However, evidence ascribed to nanoparticle-specific antimicrobial activity and/or action in synergy with Ag^+ has been adduced (Stabryla et al. 2018). The rate of dissolution depends on surface properties, which is in turn hinged on shape and surface-stabilizing molecules (Helmlinger et al. 2016). Surface passivation is also a dynamic process and the coating could change based on the molecules present in the environment and their differential affinity for the AgNP surface (Louie et al. 2016). Therefore, to enable AgNPs to reach their preferred site of action in the desired state, immense efforts have been spent on the appropriate biocompatible functionalization (Kang et al. 2019). Hence, it is important to have synthetic procedures that yield dimensional monodispersibility and discernible surface functionalization for anticipated end-use.

The solution-phase synthesis of AgNPs is widely used to produce nanoparticle with diverse shapes and sizes. Prerequisites for their successful formation are metal precursor/ion source-commonly silver nitrate ($AgNO_3$), reductant/electron donor, and a colloidal stabilizer (Hühn et al. 2017). Occasionally, the reductant, its oxidation by-products, or other arising complex serve as the colloidal stabilizers. Essentially, it is desirable to model reaction kinetics, such that one can synthesize nanoparticles of the desired shape and size by pairing the precursor with appropriate reductants (Rodrigues et al. 2018). However, the simultaneous presence of stabilizers, coordination ligands, and preformed seeds complicate attempts to fine-tune the size and

morphology of the nanoparticles (Yang et al. 2017). Consequently, most of the methodologies described in literature arise from trial and error optimization of experimental parameters, including the concentration of precursor, reductants and stabilizer, reaction temperature, and pressure. Varying the parameters can lead to a change in the shape and size of nanoparticles. This is envisaged to arise from the synergistic role of each component. Additionally, secondary reactants and products do evolve in the synthesis process (Pestov et al. 2015).

There are many publications on one-pot green synthesis of AgNPs using aqueous plant extracts. This is based on the perceived eco-friendliness of the procedures and biocompatibility of the end product. Plant extracts contain diverse molecules that act as reductants, capping agents, and coordination ligands. They include organic acids, phenolic compounds, sugars, enzymes, and cofactors (Mittal et al. 2013). However, extracts host other components that react with ionic metal precursors to yield insoluble products that cannot be removed using routine purification techniques (Ranoszek-Soliwoda et al. 2019). Moreover, it is difficult to determine the exact species passivating the surface (Manukumar et al. 2017c; Khan et al. 2018). Consequently, green synthesis is plagued by a lack of control over the production milieu, making precise control of size, shape, and surface properties difficult.

The challenges presented by green synthesis can be overcome by protocols that allow for post-synthesis modification of AgNPs. Citrate capped silver nanoparticles (CtAgNPs) offer such a synthetic route. Due to weak surface passivation by citrate, the nanoparticles can be functionalized with preferred ligands for specific application upon fabrication (Bastús et al. 2014). A combination of sodium citrate and tannic acid as reducing and stabilizing agents, with $AgNO_3$ as the metal precursor, has been used successfully to synthesize monodisperse spherical and quasi-spherical CtAgNPs (Dadosh 2009; Rainville et al. 2013; Bastús et al. 2014; Ranoszek-Soliwoda et al. 2017). Typically, sodium citrate is provided at a higher molar concentration than $AgNO_3$ and held constant in the reaction mixture, while tannic acid is varied to tune the nanoparticle size. The size reproducibility of the procedures is tied to meticulous replication of the experimental parameters. Molecules with amine and thiol groups readily displace citrate from the surface of AgNPs (Bastús et al. 2014).

Chitosan, a linear polymer of β-(1 → 4)-D-glucosamine and N-acetyl-D-glucosamine, is a biocompatible biomolecule that has been used widely in reduction and capping of silver and gold nanoparticles (Marpu and Benton 2018). It avails multiple amine groups envisaged to bind to the silver surface (Manukumar et al. 2017a, b). However, it has been noted that chitosan undergoes hydrolysis and oxidation to yield numerous products when used both as a reducer of metallic precursor ions and subsequent stabilizing agent in one-pot reactions. Carapeto et al. (2017) tracked evolved species when chitosan was employed both as a reducing and stabilizing agent and AgNO$_3$ as a silver precursor in AgNPs synthesis. They revealed that oxidation products were carbonyl groups from the oxidation of alcohol and or glycosidic groups, present in the chitosan chains. Results from a study of the mechanism of Au(III) reduction to gold nanoparticles by chitosan indicated that its hydrolysis products and not chitosan were the main reducing agents (Pestov et al. 2015). Chitosan decomposed into soluble chitosan oligomers, derivatives of glucosamine acids, and formic acid. Carapeto et al. (2017) pointed out that additional biological activity of the nanocomposites could arise from residual reactants and by-products if nanoparticles are not purified. For instance, formic acid, which was produced in appreciable quantities, is toxic to some mammalian cells and has antibacterial properties (Treichel 2004; Griggs and Jacob 2005).

Betanin (betanidin 5-O-β-Glucoside, CI Natural Red 33, E-number E162) is a natural compound mainly obtained from beetroot and approved food color (Gonçalves et al. 2012). Additionally, it has high antioxidant activity (Gliszczyńska-Świgło et al. 2006). It has been used as a reducing and capping agent for AgNPs. Fernandes et al. (2016) synthesized betanin silver nanoparticles (BtnAgNPs) using both microfluidic reactor assembly and batch system with AgNO$_3$ as the metal precursor under alkaline conditions. Pavliuk et al. (2017) in the same research group with Fernandes et al. (2016) used the optimized microfluidic synthesis system reaction conditions to synthesize BtnAgNPs as part of a nano-hybrid plasmonic photocatalyst for hydrogen production. They proposed that betanin and its alkaline hydrolysis or oxidation derivatives were the likely reducing and capping agents. Under alkaline conditions and increasing temperature, betanin is rapidly hydrolyzed to betalamic acid and 5-O-glycosylated cyclo-DOPA (Esteves et al. 2018).

Many studies on antimicrobial properties of AgNPs present several gaps that hinder comparative evaluation. They include the direct testing of as-synthesized mixtures (i.e., without removal of excess reactants), ambiguous or lack information on purification steps, absence of analytical techniques used to estimate the concentration of nanoparticles in test media, and different concentration of microbes in the final inoculum. Additionally, there are variations on the choice of assays for minimum inhibitory concentration (MIC) and minimum bactericidal concentration (MBC). The disk diffusion assay has been used in many studies to evaluate bacteria susceptibility to AgNP. However, according to Petersen et al. (2014) disk diffusion assay may not be an accurate assessment of particle toxicity when the mechanism of toxicity requires cell-particle contact. This is because differences in engineered nanomaterials (ENM) transport properties, relative to those of traditional chemicals, can cause artifacts. Moreover, due to the adsorption of particles to the filter paper and the lower diffusion coefficients of the particles when compared to conventional small-molecule antibiotics, the zone of inhibition test is likely to demonstrate artifacts when the analyte is an ENM suspension. Therefore, unless the particle concentration can be quantified in the surrounding agar, it is important to consider the disk diffusion test inappropriate.

The present study focused on initial synthesis and purification of CtAgNPs using an established technique to yield monodisperse AgNPs. This was followed by post-synthesis functionalization via ligand exchange with chitosan oligosaccharide and betanin. Particular attention was given to purification and rapid estimation of nanoparticle concentrations via ultraviolet-visible (UV-Vis) spectroscopy after correlating peak absorbance at λ_{max} with high-resolution inductively coupled plasma mass spectrometry (HR-ICP-MS) results. The nanoparticles were characterized and subsequently evaluated for antimicrobial properties against *Staphylococcus aureus* using the Clinical and Laboratory Standards Institute (CLSI) standard broth microdilution method (CLSI 2018). We provided an alternative route to the fabrication of AgNPs functionalized with defined biomolecules while building upon a reproducible particle size synthesis route.

Materials and methods

Chemicals

Sodium citrate tribasic dihydrate (Na$_3$C$_6$H$_5$O$_7$. 2H$_2$O), tannic acid (C$_{76}$H$_{52}$O$_{46}$), AgNO$_3$, Mueller-Hinton Broth (MHB), and Mueller-Hinton Agar (MHA) were from

Himedia (Mumbai, India). Betanin (diluted with dextrin) and chitosan oligosaccharide lactate (average M_n 5000, > 90% deacetylated) were procured from Sigma-Aldrich (St. Louis, MO). All chemicals were used as received without further purification. Ultrapure water (> 18.2 MΩ cm resistivity) produced by PURELAB Option-Q (ELGA LabWater, UK) was used in the preparation of all solutions. All glassware and Teflon-coated stir bars were cleaned with a detergent followed by aqua regia, thoroughly rinsed with ultrapure water, and finally, acetone.

Preparation of CtAgNPs

CtAgNPs were synthesized according to a previously reported procedure (Bastús et al. 2014). Briefly, a 100 mL aqueous solution of $Na_3C_6H_5O_7 \cdot 2H_2O$ (5.00 mM) and $C_{76}H_{52}O_{46}$ (1 mM) was brought to reflux while stirring, and then 1 mL of $AgNO_3$ (25.00 mM) was quickly injected. The mixture was cooled to room temperature, transferred to a clean sterile glass media bottle, and held in a refrigerator ($\sim$ 4 °C) before purification.

Purification of nanoparticles

To remove excess citrate and $C_{76}H_{52}O_{46}$, the as-synthesized mix of CtAgNPs was concentrated by centrifuging 1.5-mL aliquots in 1.5-mL centrifuge tubes at a 10,000 relative centrifugal force (rcf) for 10 min using RC 4100 centrifuge (Elteck, India). The supernatants were removed and the particles dispersed in 1.5 mL of 2.2 mM $Na_3C_6H_5O_7 \cdot 2H_2O$. The particles were centrifuged once more, the supernatant removed, and then re-dispersed in 2.2 mM $Na_3C_6H_5O_7 \cdot 2H_2O$. These portions were preserved as CtAgNPs under refrigeration ($\sim$ 4 °C). Before characterization and functionalization, excess citrate was removed by centrifuging the CtAgNPs at 10000 rcf for 10 min, re-dispersing in ultrapure water, and repeating the procedure once (i.e., × 2 water rinse).

UV-Vis spectroscopy characterization

UV-Vis absorbance spectra in between 300 and 800 nm were obtained at 1-nm interval using a double beam Spectrophotometer Model U-3900 (Hitachi, Japan), 2-nm slit width setting, fitted with deuterium and tungsten lamps. A 10-mm optical path quartz cuvette was used to hold portions of nanoparticle colloids against water as the reference.

Hydrodynamic diameter and zeta potential measurements

Nanotrac Wave Model MN401 (Microtrac Inc., USA) with a backscattering laser probe operating at 780 nm and mounted at a 180° angle, was used to measure AgNPs hydrodynamic diameter and zeta potential as per the manufacturer's instructions.

Transmission electron microscopy, selected area diffraction and energy dispersive spectroscopy

Briefly, a droplet of CtAgNPs was drop cast onto a carbon-coated copper grid and left to air dry. Imaging, acquisition of SAED pattern, and EDS spectrum of the CtAgNPs was done using a 200 kV high-resolution-transmission electron microscope (HR-TEM) model JEM 2100F (Jeol, Japan). ImageJ 1.52n National Institutes of Health, USA (Schneider et al. 2012) was used to process TEM images, count, and measure the sizes of the nanoparticles. Get dSpace plugin for ImageJ was used to calculate the interplanar spacing (d) in Angstroms (Å) from the Gatan's format diffraction patterns for Indexing. Microsoft Excel 2010 (Microsoft Corporation, Redmond, WA, USA) with data analysis add-ins was used to compute descriptive statistics and summarize the size distribution in a histogram.

Silver concentration analysis

The concentration of Ag in the purified nanoparticle dispersion was determined by HR-ICP-MS using an ELEMENT XR spectrometer (Thermo Fisher Scientific, Germany). Briefly, a 5% vol nitric acid (HNO_3) mixture was made by diluting HNO_3 (Sigma-Aldrich, > 99.999% trace metal basis) with water. Unknown Ag concentrations were determined by comparison to a 5-point standard curve with a range of 1–100 ppb prepared from an Ag standard for ICP (Merck, Certipur® 1000 mg/L Ag in HNO_3) diluted in the 5% HNO_3 matrix. Nanoparticle dispersion samples were also appropriately diluted with 5% HNO_3. The standards and unknown samples were integrated for 2 min and 3 readings taken automatically. To ensure the removal of all residual metals from the instrument, a 5-min flush time with the 5% HNO_3 solution was employed

between runs, and a blank analyzed before each unknown sample.

Estimation of the number of nanoparticles in solution was carried out as described by Hühn et al. (2017). Briefly, the mean diameter from TEM was used to calculate the volume of the nanoparticles. Consequently, the mass of each core was gotten by multiplying the density of Ag by volume. To estimate the number of nanoparticles per liter, the total Ag mass in solution from HR-ICP-MS results was divided by the mass of the nanoparticle core. Based on silver concentration obtained via HR-ICP-MS, a calibration curve of absorbance at LSPR λ_{max} against varying concertation of nanoparticle dispersion was derived for quick estimation of Ag concentrations to be incorporated into bacterial growth media.

Ligands amount determination

To calculate the amount of capping agent to be added for ligand exchange and avail enough molecules to cover the surface of the nanoparticles, while providing for an excess amount, an assumption of 5 ligands per nm^2 was made and a $\times 20$ excess provided in the solution. This was considered appropriate based on previous studies using one thiol moiety liner ligands on AgNPs. For instance, Johnston et al. (2016) determined the capping density of poly(ethylene glycol) methyl ether thiol (average MW = 1000 Da) to be 2.11 ± 0.06 ligands per nm^2 on 25.4 ± 2.1 nm diameter AgNPs using ^1H nuclear magnetic resonance analysis, while Amoli et al. (2012) arrived at a density of 6.4 ligands per nm^2 of 11-mercaptoundecanoic acid (MW = 218.36) on 4.5 ± 1.3 nm diameter AgNPs using thermogravimetric analysis.

Ligand exchange with betanin

To produce BtnAgNPs 50 μL of 0.5 mM aqueous solution of betanin solution was added to 1 mL of CtAgNP solutions purified as described above, having an absorbance of 0.5 at λ_{max} of 432 nm when diluted at a 0.5 ratio, with an estimated concentration of 3.3×10^{10} AgNPs/mL in 1.5 mL centrifuge tubes. The mixture was shaken in darkness for 12 h at room temperature using a tube rocker. Immediately after this mixing time, the particles were centrifuged at 10000 rcf for 10 min and the supernatant with excess betanin and decanted. The pellets were washed with 1 mL nano-pure H_2O to remove excess betanin and displaced citrate, centrifuged and re-dispersed in water for characterization. Surface passivation changes were monitored using UV-Vis spectroscopy and zeta potential.

Ligand exchange with chitosan oligosaccharide

Chitosan oligosaccharide bears multiple primary amino groups; the method used by Bastús et al. (2016) was used with slight modification. Briefly, a 0.25 mM aqueous solution of chitosan oligosaccharide lactate (average M_n 5000) was prepared using ultrapure water. Ten microlitres of the chitosan solution were added to 1 mL of CtAgNPs solutions purified as described above and with an estimated 3.3×10^{10} AgNPs/mL. The mixture was kept in the dark under vigorous rocking for 12 h. The functionalized NPs were centrifuged to remove the unbound molecules and re-dispersed in an equivalent volume of ultrapure water to yield chitosan oligosaccharide stabilized AgNPs (CHTAgNPs) and taken for characterization. UV-Vis spectroscopy and zeta potential were used to monitor functionalization. All the surface-modified nanoparticles were kept under refrigeration at ∼ 4 °C during the experimental duration. The stability from aggregation was monitored by evaluating the UV-Vis spectra of the nanoparticles.

Antimicrobial analysis

CLSI standard broth microdilution method was used to check for the antibacterial activity of the nanoparticles (CLSI 2018). Briefly, 50 μL aliquots of sterile MHB were dispensed into columns 1 to 11 of 96 well flat-bottom plates. A 100 μL nanoparticle colloid at 100 ppm silver (obtained from centrifugal concentration of citrate, oligochitosan, and betanin functionalized AgNPs) was put into column 12 wells and twofold serial dilutions done to yield a final test range of in between 50.00 and 0.05 ppm in between columns 12 and 2. Column 1 was reserved for negative control with no AgNP treatment. Ionic silver (Ag^+) from $AgNO_3$ at corresponding ppm was used as the positive control. Four typical colonies of *Staphylococcus aureus* ATCC 12600 were picked with a loop from an overnight culture on MHA streak plate, dispersed into 2 mL of MHB in a round-bottomed culture tube and vortexed to evenly distribute the cells. The optical density of the bacterial suspension was adjusted to between 0.08 and 0.1 at 625 nm in sterile disposable plastic cuvettes. A 1:150

dilution was made to yield approximately 1×10^6 CFU/mL. Fifty microliters of the bacterial suspensions were added into the aliquots of diluted AgNPs, to give a final inoculum of 5×10^5 CFU/mL in 100 μL of the final aliquot in each well. The plates were covered with Parafilm®, incubated at 37 °C, and visually examined for growth after 24 h. Tests were conducted in triplicates and repeated twice.

Results and discussion

Using the method developed by Bastús et al. (2014), we produced nanoparticles by injecting 1 mL of AgNO₃ (25.00 mM) into a 100 mL boiling aqueous solution of $Na_3C_6H_5O_7 \cdot 2H_2O$ (5.00 mM) and $C_{76}H_{52}O_{46}$ (1 mM). Upon adding AgNO₃, the color of the mixture transformed from transparent light yellow to dark yellow within a few seconds, indicating formation of AgNPs. The nanoparticles were purified by centrifugation and then re-dispersed in 2.2 mM $Na_3C_6H_5O_7 \cdot 2H_2O$ for storage and characterization. UV-Vis spectroscopy, HR-TEM, dynamic light scattering (DLS), and zeta potential analysis were used to characterize the nanoparticles. HR-ICP-MS revealed the concentration of silver. The CtAgNPs were then modified via ligand exchange to produce BtnAgNPs and CHTAgNPs. Lastly, the nanoparticles were tested for bactericidal effect on *S. aureus*.

The characterization results of purified CtAgNPs are summarized in Fig. 1. They exhibited a LSPR λ_{max} peak at 432 nm and had a full width at half-maximum (FWHM) of 95 nm (Fig. 1a). The nanoparticles were roughly spherical as depicted on the TEM image (Fig. 1f) with a mean size of 37.9 ± 8.6 nm. DLS analysis gave a slightly higher average diameter of 39.1 ± 7.2 nm. Zeta potential of the nanoparticles was -32 mV. A monomodal distribution was displayed by the two sizing techniques (Fig. 1b, c). The combined use of $C_{76}H_{52}O_{46}$ and $Na_3C_6H_5O_7$ as reducing and stabilizing agents to produce AgNPs has been hailed as a reproducible method for the production of size-tunable nanoparticles, whose surface coating can be easily functionalized, because of the loose electrostatic stabilization by citrate (Hühn et al. 2017). Bastús et al. (2014) produced nanoparticles with a diameter of 36.9 ± 6.2 nm, using a similar ratio of reactants that we sort to replicate in the present study. We achieved a diameter of 37.9 ± 8.6 nm. The precision of the method was also demonstrated by Hühn et al. (2017) who produced CtAgNPs with a

diameter of 15 ± 1 nm, using similar parameters employed by Bastús et al. (2014) to yield 14.8 ± 1.4 nm. Adherence to the synthesis protocol is essential for reproducibility and minimal alterations to the reaction parameters can cause variations. For instance, utilizing a similar ratio of reactants used by Bastús et al. (2014) to yield 10 ± 0.9 nm CtAgNPs, Barbalinardo et al. (2018) slightly varied the procedure by refluxing the reaction mixture for 30 min instead of immediate cooling after addition of AgNO₃, producing 15 ± 3 nm diameter CtAgNPs. Though not provided in most publications, FWHM of the UV-Vis spectrum can be an important indicator of the nanoparticle size dispersion (Rainville et al. 2013). Figure 1e shows the SAED pattern images demonstrating the crystalline nature of the AgNPs. Calculated *d* space values of the electron diffraction image were 2.365, 2.044, 1.457, and 1.225 Å. The *d* values were indexed to the corresponding (111), (200), (220), and (311) *hkl* crystal planes of face-centered cubic (fcc) structure of crystalline silver (Edington 1975). The presence of elemental silver was also confirmed by EDS, shown by the peak at 3 keV (Fig. 1d).

The concentration of silver in the purified CtAgNPs reconstituted to an identical volume to the as-synthesized mixture with water upon centrifugal purification was 20.3 ppm, as determined by HR-ICP-MS. The precursor Ag⁺ concentration in the synthesis solution was ≈27.0 ppm. This gave a yield of 75% on Ag mass basis. Using the average diameter of 37.9 nm, the estimated volume, mass, and the surface area of each nanoparticle core were 2.88×10^4 nm³, 2.99×10^{-16} g, and 4.51×10^3 nm², respectively, translating to an approximate count of 6.79×10^{10} AgNPs/mL in the purified colloid. The nanoparticle dispersion giving a concentration of 20.3 ppm presented an absorbance of 2.441 at LSPR λ_{max} 432 nm. Figure 2 shows a calibration curve obtained from plotting varying concentrations of Ag colloids against their absorbance at λ_{max} 432 nm. A good linear dynamic range was obtained within the plotted range. The curve was used to approximate the Ag concentration of centrifugal concentrated nanoparticle colloids used in antimicrobial tests. An excellent linear relationship between Ag concentration and absorbance at λ_{max} for AgNPs has been observed in other studies, supporting its use in estimating silver concentration in colloids (Zook et al. 2011; Paramelle et al. 2014; Johnston et al. 2018). Notably, the final concentration of the purified nanoparticles was close to the amount of silver (0.02 mg/mL = 20 ppm) in Nanoexact™ range of silver colloids sold by Nanocomposix, a vendor of CtAgNPs. To corroborate our observation, we followed
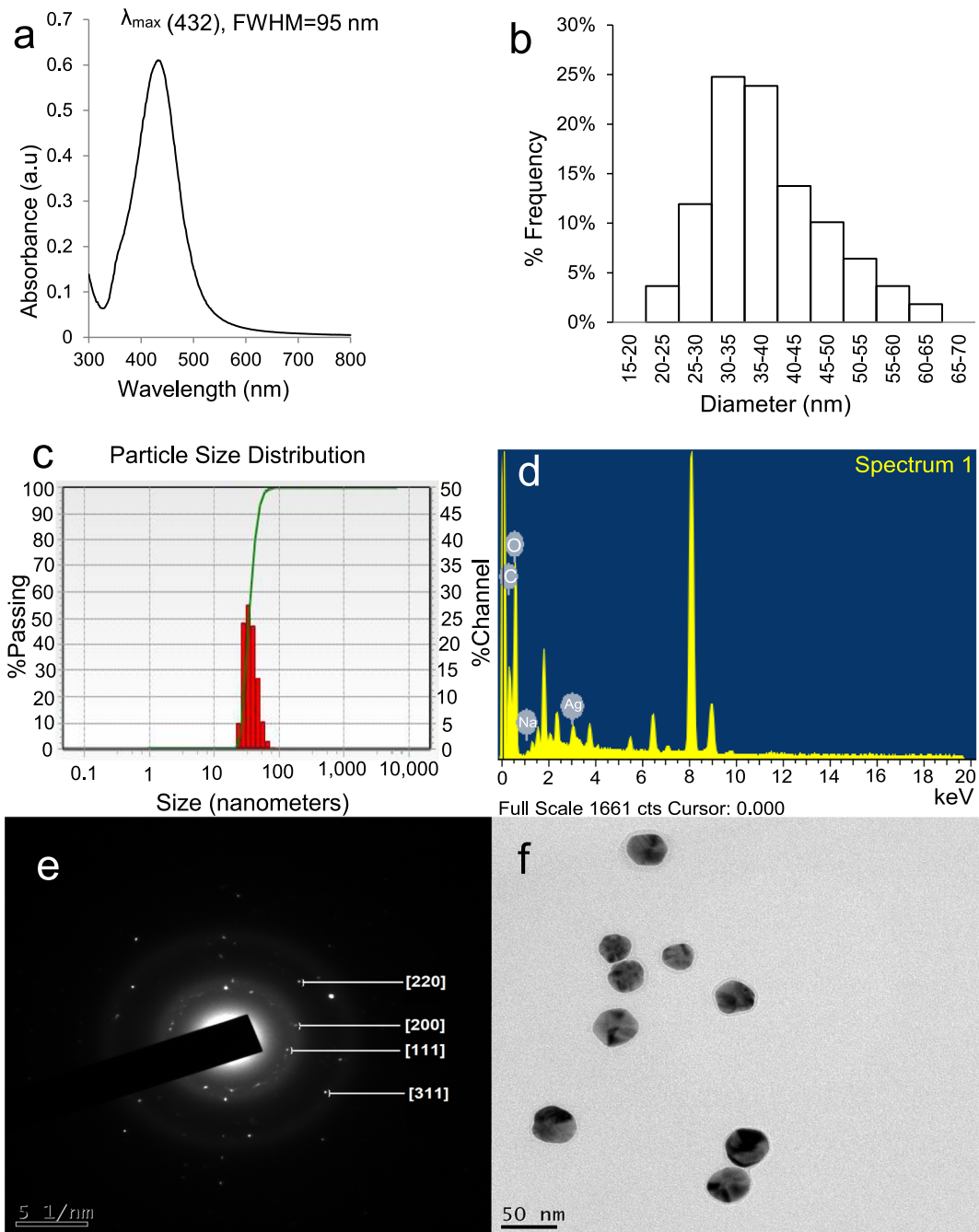
Fig. 1 Representative data of CtAgNPs obtained by injecting 1 mL of 25 mM AgNO₃ into a boiling 100 mL aqueous solution of 1 mM tannic acid and 5 mM sodium citrate. **a** UV-Vis spectrum; **b** TEM size distribution histograms for the nanoparticles (mean diameter 37.9 ± 8.6 nm); **c** DLS size distribution of Ag NPs (mean diameter 39.1 ± 7.2 nm), the *x*-axis displays size on a logarithmic scale, the solid line plot gives the cumulative percent, while the bar graph depicts the percent between sizes; **d** energy dispersive spectroscopy (EDS) spectrum of the CtAg NPs, Ag peak appears at 3 keV; **e** SAED pattern of the AgNPs showing representative spots indexed to *hkl* crystal planes of fcc structure of crystalline silver; **f** TEM microscopy image of the nanoparticles

their prescribed protocol to evaluate the stability of CtAgNPs, i.e., diluting the nanoparticle colloid at a ratio of 1:2 (colloid: water) and obtaining a UV-Vis spectrum of

the colloid (Nanocomposix 2012). Nanoparticle dimensions outlined in the guidelines (10–100 nm) were plotted against the provided expected peak absorbance ranges and
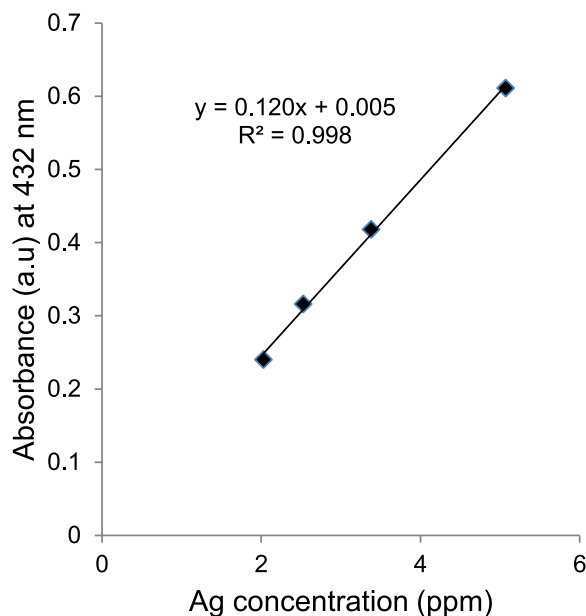
Fig. 2 Calibration curve for estimating Ag in nanoparticle colloids. The chart was obtained by plotting the absorbance (at LSPR λ_{max} 432 nm) against known concentrations of CtAgNPs. Concentrations were derived from appropriate dilutions of the 20.3 ppm Ag (HR-ICP-MS analysis) nanoparticle dispersion. Insets are results of regression analysis showing a strong linear relationship
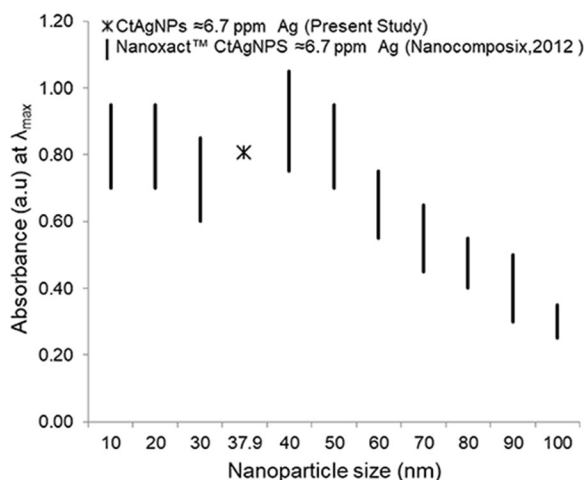

Fig. 3 Comparison of absorbance intensity of CtAgNPs colloids with identical Ag mass concentration but different sizes. The vertical bars represent upper and lower prescribed absorbance range for varying sizes (10–100 nm) at corresponding LSPR λ_{max} of *Nanoxact ™* CtAgNPs (20.0 ppm Ag mass) diluted at a 1:2 ratio colloid: water (≈ 6.7 ppm) as given in *Protocol for testing Nanoxact ™ silver nanoparticles stability: UV/Visible spectroscopy* in *Guidelines for nanotoxicology researchers using nanocomposix materials* (Nanocomposix 2012). The asterisk (*) shows the absorbance of purified CtAgNP colloids obtained in the present study, 37.9 nm in diameter, and 20.3 ppm Ag concentration diluted at a colloid: water ratio of 1:2 (≈ 6.7 ppm)

a comparison with our colloid peak value at λ_{max} made. The results are presented in Fig. 3 and indicate the relative correspondence of the absorbance intensity of our nanoparticles to those of a nearby diameter of 40 nm. In our study, functionalization did not change the absorbance intensity alongside the observed slight redshift in the λ_{max} of the modified nanoparticles. Therefore, Ag concentration estimates for BtnAgNPs and CHTAgNPs used in antimicrobial tests were done using the same calibration curve. As noted by Paramelle et al. (2014), where a capping does not lead to loss or agglomeration of nanoparticles, a direct calibration can be made against that of the initial nanoparticles to estimate the AgNP concentration.

UV-Vis spectrum in between 300 and 800 nm was used to check for ligand exchange and long-term stability. There was a redshift of the LSPR λ_{max} peak from 432 nm, to 434 nm and 437 nm for CHTAgNPs and BtnAgNPs, respectively (Fig. 4). No second plasmon bands were observed at a higher wavelength, signifying the absence of nanoparticle aggregation during ligand exchange. A redshift of LSPR λ_{max} peak upon the functionalization of AgNPs is a common phenomenon associated with an alteration on the dialectic constant of

the medium surrounding the nanoparticle (Shen et al. 2013). Similar LSPR λ_{max} peak changes have been noted by other authors (Bastús et al. 2016; Barbalinardo et al. 2018) upon change of capping on CtAgNPs. This provides a quick way to monitor a change in capping and stability of the AgNPs. Further surface modifications were confirmed by a change of zeta potential from -32 mV on CtAgNPs to -28 mV and $+26$ mV for BtnAgNPs and CHTAgNPs, respectively (Table 1). Zeta potential also helps to predict the stability of a nanodispersion. Dispersion with a zeta potential of ± 20–30 mV and $> \pm 30$ mV are considered moderately stable and highly stable, respectively, whereas those with values in the range of between -10 and $+10$ mV are considered neutral, meaning that the particles will eventually settle out (Clogston and Patri 2011; Bhattacharjee 2016). All nanoparticles remained stable to aggregation for 6 months during the experiments.

Betanin has two amine groups in its structure. Above neutral pH, betanin is postulated to exist as a tri-anion with all the carboxyl groups deprotonated (Frank et al. 2005; Gliszczyńska-Świgło et al. 2006). Silver has a higher affinity for amines compared to carboxyl groups
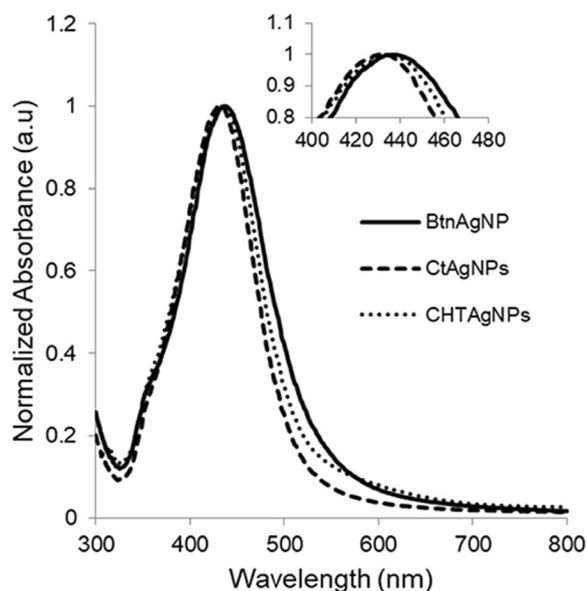
Fig. 4 UV-Vis spectra showing changes upon the functionalization of NPs. CtAgNPs (black dashed) line obtained before ligand exchange, CHTAgNPs (dotted line), and BtnAgNPs (solid line) and after the ligand exchange process with chitosan and betanin respectively. Inset is an expanded highlight of the peak maxima showing a redshift once the native molecules are replaced by chitosan and betanin

(Bell and Kramer 1999; Baalousha et al. 2018). Therefore, it is proposed that betanin most likely adsorbed to AgNPs with the amine groups conferring an overall negative charge. On the other hand upon dissolution, the water-soluble chitosan oligosaccharide lactate yields chitosan oligomers with multiple amine groups suggested to bind to the silver nanoparticle and also provide overall positive charge. Amines stabilize metal nanoparticle stabilizers via coordination of the lone pair of electrons on nitrogen atoms (Rodrigues et al. 2018). Additionally, the presence of multiple amine groups gives higher stability constants (Baalousha et al. 2018). A recent study by Barbosa et al. (2019) on the

ionization behavior of polymers using zeta potential showed that medium molecular chitosan (75–85% deacetylation) had a zeta potential of approximately + 20 mV at around neutral pH. The higher degree of deacetylation (> 90%) of chitosan oligosaccharide used in this study would possibly provide more ionizable groups on chains coating the nanoparticles and hence the observed higher positive (+ 26 mV) magnitude of zeta potential. Depending on the concentration, macromolecules such as chitosan are proposed to adopt varying conformations on the AgNP surfaces, e.g., end-grafted brush-like, loop, pancake, mushroom, or even composites, where AgNPs are bridged by the polymer chains and occluded in the matrix (Louie et al. 2016; Carapeto et al. 2017).

The bactericidal effect of the nanoparticles fabricated in this study is summarized in Table 2. CtAgNPs, CHTAgNPs, and BtnAgNPs had a similar MIC of 12.5 ppm while Ag^+ inhibited *S. aureus* at 6.25 ppm. An antimicrobial evaluation using commercial 60 nm CtAgNPs and 40 nm CtAgNPs (as-synthesized mixture) generated via sodium citrate reduction on a wide range of reference and multidrug-resistant *S. aureus* strains gave MIC of ≥ 10 and 6.7–13.5 ppm Ag, respectively (Cavassin et al. 2015). For CtAgNPs generated in the aforementioned studies, there was an apparent assumption that all Ag^+ was converted to nanoparticles and no purification step was documented. Therefore, there is a probability that ionic silver could have contributed to bactericidal action. The size, nanoparticle surface chemistry, and type of broth media used in the antimicrobial test are other factors that influence MIC of AgNPs on bacteria (Greulich et al. 2012; Helmlinger et al. 2016; Johnston et al. 2018). This diversity creates a challenge when attempting to make a comparison amongst different studies. Nevertheless, from a general perspective,

Table 1 Zeta potential of AgNPs based on changes in surface functionalization

Nanoparticles	Zeta potential (mV)
Citrate stabilized (CtAgNPs)	− 32
Betanin stabilized (BtnAgNPs)	− 28
Chitosan oligosaccharide stabilized (CHTAgNPs)	+ 26

Indicated zeta potential is an average generated from an instrument setting of 3 runs of 90 s per sample

Table 2 Minimum inhibitory concentrations (MIC) of Ag^+ from silver nitrate and silver nanoparticles on *Staphylococcus aureus* ATCC 12600 in Mueller-Hinton Broth (MHB)

Ag source (N = 3)	MIC/ppm (Ag^+/Ag^0)
Silver nitrate	6.25 (Ag^+)
Citrate stabilized (CtAgNPs)	12.5
Betanin stabilized (BtnAgNPs)	12.5
Chitosan oligosaccharide stabilized (CHTAgNPs)	12.5

Tabulated values indicate consistently observed MICs for tests conducted in triplicates and repeated twice

the antimicrobial activity of AgNPs with similar capping increases with an increase in the surface area, suggesting that Ag^+ is the main bactericidal species (Helmlinger et al. 2016). The composition of liquid growth media also has an impact on bacterial growth kinetics. A recent test on the antibacterial effect of Ag^+ on *Bacillus subtilis* revealed decreased toxicity where media contained tryptone, yeast extract, or S^{2-} (De Leersnyder et al. 2018). Formation of a protein corona upon contact of AgNPs with media proteins is another aspect that has been shown modulate nanoparticle toxicity (Durán et al. 2015). Though broth chemistry regulates ionic silver release, the dynamics are complex necessitating independent assessment of different media (Johnston et al. 2018). AgNPs functionalized with organothiol groups have reduced toxicity when compared to those capped with molecules bearing amine and carboxylate stabilizers. Thiol (R-SH) moiety bearing stabilizers bind strongly to AgNPs limiting oxidation and hence slower release of Ag^+ and a lower antimicrobial effect (Le Ouay and Stellacci 2015). For almost similar sized AgNPs (≈ 7 nm), cysteine-AgNPs had a MIC of 580 μM Ag (62.6 ppm) when compared against 69 μM (7.4 ppm) of poly(vinylpyrrolidone)-AgNPs on *S. aureus* in MHB (Padmos et al. 2015).

Conclusions

Whereas the biomolecules, i.e., betanin and chitosan (with varying molecular weight degree and degree of deacetylation), used in this study have been applied previously in synthesis and stabilization AgNPs, our investigations took a different approach by using them post-synthesis as stabilizers via ligand exchange. Additionally, to the best of our knowledge based on literature search, the use of the commercial chitosan oligosaccharide (Average M_n 5000) has not been applied elsewhere for AgNP surface capping. The two biomolecules stabilized the AgNPs in a weak adsorption mode on the metal surface characteristic of carboxylate and amine bearing stabilizers.

Sodium citrate and tannic acid are inexpensive molecules that are widely and safely used at appropriate concentrations in the food industry and medical fields. Their ability to yield reproducible size AgNPs has been reaffirmed. This is a recommendable procedure for future comparative studies based on similar-sized nanoparticles as opposed to having a multitude of

investigations with standalone inferences. Similarly, more trials on successful stabilization of AgNPs with purified biomolecules for bactericidal use can be carried out. It is also evident from these studies and other investigations that not all Ag^+ are reduced to Ag^0. Consequently, the use of as-synthesized colloids could give erroneous conclusions on the bactericidal activity of the AgNPs. Therefore, a purification step is vital. The strong LSPR at corresponding λ_{max} for AgNPs provided a sensitive estimation of Ag^0 within the MIC range encountered in present studies and can be exploited routinely for quantifying elemental silver concentration in antimicrobial tests.

Compliance with ethical standards

Conflict of interest   The authors declare that they have no competing interests.

References

Amoli BM, Gumfekar S, Hu A, Zhou YN, Zhao B (2012) Thiocarboxylate functionalization of silver nanoparticles: effect of chain length on the electrical conductivity of nanoparticles and their polymer composites. J Mater Chem 22: 20048–20056. https://doi.org/10.1039/C2JM33280A

Baalousha M, Afshinnia K, Guo L (2018) Natural organic matter composition determines the molecular nature of silver nanomaterial-NOM corona. Environ Sci Nano 5:868–881. https://doi.org/10.1039/C8EN00018B

Barbalinardo M, Caicci F, Cavallini M, Gentili D (2018) Protein corona mediated uptake and cytotoxicity of silver nanoparticles in mouse embryonic fibroblast. Small 14:1801219. https://doi.org/10.1002/smll.201801219

Barbosa JAC, Abdelsadig MSE, Conway BR, Merchant HA (2019) Using zeta potential to study the ionisation behaviour of polymers employed in modified-release dosage forms and estimating their pKa. Int J Pharm 1:100024. https://doi.org/10.1016/j.ijpx.2019.100024

Barillo DJ, Marx DE (2014) Silver in medicine: a brief history BC 335 to present. Burns 40:S3–S8. https://doi.org/10.1016/j.burns.2014.09.009

Bastús NG, Merkoçi F, Piella J, Puntes V (2014) Synthesis of highly monodisperse citrate-stabilized silver nanoparticles of up to 200 nm: kinetic control and catalytic properties. Chem Mater 26:2836–2846. https://doi.org/10.1021/cm500316k

Bastús NG, Piella J, Puntes V (2016) Quantifying the sensitivity of multipolar (dipolar, quadrupolar, and qctapolar) surface plasmon resonances in silver nanoparticles: the effect of size, composition, and surface coating. Langmuir 32:290–300. https://doi.org/10.1021/acs.langmuir.5b03859

Bell RA, Kramer JR (1999) Structural chemistry and geochemistry of silver-sulfur compounds: critical review. Environ Toxicol Chem 18:9–22. https://doi.org/10.1002/etc.5620180103

Bhattacharjee S (2016) DLS and zeta potential – what they are and what they are not? J Control Release 235:337–351. https://doi.org/10.1016/j.jconrel.2016.06.017

Carapeto AP, Ferraria AM, do Rego AMB (2017) Unraveling the reaction mechanism of silver ions reduction by chitosan from so far neglected spectroscopic features. Carbohydr Polym 174:601–609. https://doi.org/10.1016/j.carbpol.2017.06.100

Cavassin ED, de Figueiredo LFP, Otoch JP, Seckler MM, de Oliveira RA, Franco FF, Marangoni VS, Zucolotto V, Levin ASS, Costa SF (2015) Comparison of methods to detect the in vitro activity of silver nanoparticles (AgNP) against multidrug resistant bacteria. J Nanobiotechnol 13:64. https://doi.org/10.1186/s12951-015-0120-6

Chernousova S, Epple M (2013) Silver as antibacterial agent: ion, nanoparticle, and metal. Angew Chem Int Ed 52:1636–1653. https://doi.org/10.1002/anie.201205923

Chopra I (2007) The increasing use of silver-based products as antimicrobial agents: a useful development or a cause for concern? J Antimicrob Chemother 59:587–590. https://doi.org/10.1093/jac/dkm006

Clogston JD, Patri AK (2011) Zeta potential measurement. In: McNeil SE (ed) Characterization of nanoparticles intended for drug delivery. Humana Press, Totowa, pp 63–70

CLSI (2018) Methods for dilution antimicrobial susceptibility tests for bacteria that grow aerobically CLSI standard M07, 11th edn. Clinical and Laboratory Standards Institute, Wayne

Dadosh T (2009) Synthesis of uniform silver nanoparticles with a controllable size. Mater Lett 63:2236–2238. https://doi.org/10.1016/j.matlet.2009.07.042

De Leersnyder I, De Gelder L, Van Driessche I, Vermeir P (2018) Influence of growth media components on the antibacterial effect of silver ions on *Bacillus subtilis* in a liquid growth medium. Sci Rep 8:9325. https://doi.org/10.1038/s41598-018-27540-9

Desireddy A, Conn BE, Guo J, Yoon B, Barnett RN, Monahan BM, Kirschbaum K, Griffith WP, Whetten RL, Landman U, Bigioni TP (2013) Ultrastable silver nanoparticles. Nature 501:399–402. https://doi.org/10.1038/nature12523

Durán N, Silveira CP, Durán M, Martinez DST (2015) Silver nanoparticle protein corona and toxicity: a mini-review. J Nanobiotechnol 13:55. https://doi.org/10.1186/s12951-015-0114-4

Edington JW (1975) Electron diffraction in the electron microscope, monographs in practical electron microscopy in materials science, vol 2. philips technical library. Macmillan Press, London

Esteves LC, Pinheiro AC, Pioli RM, Penna TC, Baader WJ, Correra TC, Bastos EL (2018) Revisiting the mechanism of hydrolysis of betanin. Photochem Photobiol 94:853–864. https://doi.org/10.1111/php.12897

Fernandes DLA, Paun C, Pavliuk MV, Fernandes AB, Bastos EL, Sá J (2016) Green microfluidic synthesis of monodisperse silver nanoparticles via genetic algorithm optimization. RSC Adv 6:95693–95697. https://doi.org/10.1039/C6RA20877K

Frank T, Stintzing FC, Carle R, Bitsch I, Quaas D, Straß G, Bitsch R, Netzel M (2005) Urinary pharmacokinetics of betalains following consumption of red beet juice in healthy humans. Pharmacol Res 52:290–297. https://doi.org/10.1016/j.phrs.2005.04.005

Gliszczyńska-Świgło A, Szymusiak H, Malinowska P (2006) Betanin, the main pigment of red beet: molecular origin of its exceptionally high free radical-scavenging activity. Food Addit Contam 23:1079–1087. https://doi.org/10.1080/02652030600986032

Gonçalves LCP, Trassi MA d S, Lopes NB et al (2012) A comparative study of the purification of betanin. Food Chem 131:231–238. https://doi.org/10.1016/j.foodchem.2011.08.067

Greulich C, Braun D, Peetsch A, Diendorf J, Siebers B, Epple M, Köller M (2012) The toxic effect of silver ions and silver nanoparticles towards bacteria and human cells occurs in the same concentration range. RSC Adv 2:6981. https://doi.org/10.1039/c2ra20684f

Griggs JP, Jacob JP (2005) Alternatives to antibiotics for organic poultry production. J Appl Poult Res 14:750–756. https://doi.org/10.1093/japr/14.4.750

Helmlinger J, Sengstock C, Groß-Heitfeld C, Mayer C, Schildhauer TA, Köller M, Epple M (2016) Silver nanoparticles with different size and shape: equal cytotoxicity, but different antibacterial effects. RSC Adv 6:18490–18501. https://doi.org/10.1039/C5RA27836H

Hühn J, Carrillo-Carrion C, Soliman MG, Pfeiffer C, Valdeperez D, Masood A, Chakraborty I, Zhu L, Gallego M, Yue Z, Carril M, Feliu N, Escudero A, Alkilany AM, Pelaz B, del Pino P, Parak WJ (2017) Selected standard protocols for the synthesis, phase transfer, and characterization of inorganic colloidal nanoparticles. Chem Mater 29:399–461. https://doi.org/10.1021/acs.chemmater.6b04738

Johnston KA, Smith AM, Marbella LE, Millstone JE (2016) Impact of as-synthesized ligands and low-oxygen conditions on silver nanoparticle surface functionalization. Langmuir 32:3820–3826. https://doi.org/10.1021/acs.langmuir.6b00232

Johnston KA, Stabryla LM, Smith AM, Gan XY, Gilbertson LM, Millstone JE (2018) Impacts of broth chemistry on silver ion release, surface chemistry composition, and bacterial cytotoxicity of silver nanoparticles. Environ Sci Nano 5:304–312. https://doi.org/10.1039/C7EN00974G

Kang H, Buchman JT, Rodriguez RS, Ring HL, He J, Bantz KC, Haynes CL (2019) Stabilization of silver and gold nanoparticles: preservation and improvement of plasmonic functionalities. Chem Rev 119:664–699. https://doi.org/10.1021/acs.chemrev.8b00341

Khan M, Shaik MR, Adil SF, Khan ST, al-Warthan A, Siddiqui MRH, Tahir MN, Tremel W (2018) Plant extracts as green reductants for the synthesis of silver nanoparticles: lessons from chemical synthesis. Dalton Trans 47:11988–12010. https://doi.org/10.1039/C8DT01152D

Le Ouay B, Stellacci F (2015) Antibacterial activity of silver nanoparticles: a surface science insight. Nano Today 10: 339–354. https://doi.org/10.1016/j.nantod.2015.04.002

Lee K-S, El-Sayed MA (2006) Gold and silver nanoparticles in sensing and imaging: sensitivity of plasmon response to size, shape, and metal composition. J Phys Chem B 110:19220–19225. https://doi.org/10.1021/jp062536y

Louie SM, Tilton RD, Lowry GV (2016) Critical review: impacts of macromolecular coatings on critical physicochemical processes controlling environmental fate of nanomaterials. Environ Sci Nano 3:283–310. https://doi.org/10.1039/C5EN00104H

Manukumar HM, Chandrasekhar B, Rakesh KP, Ananda AP, Nandhini M, Lalitha P, Sumathi S, Qin HL, Umesha S (2017a) Novel T-C@AgNPs mediated biocidal mechanism against biofilm associated methicillin-resistant Staphylococcus aureus (Bap-MRSA) 090, cytotoxicity and its molecular docking studies. MedChemComm 8:2181–2194. https://doi.org/10.1039/C7MD00486A

Manukumar HM, Umesha S, Kumar HNN (2017b) Promising biocidal activity of thymol loaded chitosan silver nanoparticles (T-C@AgNPs) as anti-infective agents against perilous pathogens. Int J Biol Macromol 102:1257–1265. https://doi.org/10.1016/j.ijbiomac.2017.05.030

Manukumar HM, Yashwanth B, Umesha S, Venkateswara Rao J (2017c) Biocidal mechanism of green synthesized thyme loaded silver nanoparticles (GTAgNPs) against immune evading tricky methicillin-resistant Staphylococcus aureus 090 (MRSA090) at a homeostatic environment. Arab J Chem:S1878535217301880. https://doi.org/10.1016/j.arabjc.2017.09.017

Marpu S, Benton E (2018) Shining light on chitosan: a review on the usage of chitosan for photonics and nanomaterials research. Int J Mol Sci 19:1795. https://doi.org/10.3390/ijms19061795

Mcmahon MD, Lopez R, Meyer HM et al (2005) Rapid tarnishing of silver nanoparticles in ambient laboratory air. Appl Phys B Lasers Opt 80:915–921. https://doi.org/10.1007/s00340-005-1793-6

Mittal AK, Chisti Y, Banerjee UC (2013) Synthesis of metallic nanoparticles using plant extracts. Biotechnol Adv 31:346–356. https://doi.org/10.1016/j.biotechadv.2013.01.003

Nanocomposix (2012) Guidelines for nanotoxicology researchers using nanocomposix materials. https://cdn.shopify.com/s/files/1/0257/8237/files/nanoComposix_Guidelines_for_Nanotox_Researchers.pdf?13692. Accessed 6 Mar 2020

Padmos JD, Boudreau RTM, Weaver DF, Zhang P (2015) Impact of protecting ligands on surface structure and antibacterial activity of silver nanoparticles. Langmuir 31:3745–3752. https://doi.org/10.1021/acs.langmuir.5b00049

Paramelle D, Sadovoy A, Gorelik S, Free P, Hobley J, Fernig DG (2014) A rapid method to estimate the concentration of citrate capped silver nanoparticles from UV-visible light spectra. Analyst 139:4855–4861. https://doi.org/10.1039/C4AN00978A

Pavliuk MV, Fernandes AB, Abdellah M, Fernandes DLA, Machado CO, Rocha I, Hattori Y, Paun C, Bastos EL, Sá J (2017) Nano-hybrid plasmonic photocatalyst for hydrogen production at 20% efficiency. Sci Rep 7:8670. https://doi.org/10.1038/s41598-017-09261-7

Pestov A, Nazirov A, Modin E, Mironenko A, Bratskaya S (2015) Mechanism of Au(III) reduction by chitosan: comprehensive study with ^{13}C and ^{1}H NMR analysis of chitosan degradation products. Carbohydr Polym 117:70–77. https://doi.org/10.1016/j.carbpol.2014.09.030

Petersen EJ, Henry TB, Zhao J, MacCuspie RI, Kirschling TL, Dobrovolskaia MA, Hackley V, Xing B, White JC (2014) Identification and avoidance of potential artifacts and misinterpretations in nanomaterial ecotoxicity measurements. Environ Sci Technol 48:4226–4246. https://doi.org/10.1021/es4052999

Phan HT, Haes AJ (2019) What does nanoparticle stability mean? J Phys Chem C 123:16495–16507. https://doi.org/10.1021/acs.jpcc.9b00913

Rainville L, Dorais M-C, Boudreau D (2013) Controlled synthesis of low polydispersity Ag@SiO2 core–shell nanoparticles for use in plasmonic applications. RSC Adv 3:13953. https://doi.org/10.1039/c3ra41677a

Ranoszek-Soliwoda K, Tomaszewska E, Małek K, Celichowski G, Orlowski P, Krzyzowska M, Grobelny J (2019) The synthesis of monodisperse silver nanoparticles with plant extracts. Colloids Surf B 177:19–24. https://doi.org/10.1016/j.colsurfb.2019.01.037

Ranoszek-Soliwoda K, Tomaszewska E, Socha E, Krzyczmonik P, Ignaczak A, Orlowski P, Krzyzowska M, Celichowski G, Grobelny J (2017) The role of tannic acid and sodium citrate in the synthesis of silver nanoparticles. J Nanopart Res 19:273. https://doi.org/10.1007/s11051-017-3973-9

Rodrigues TS, Zhao M, Yang T et al (2018) Synthesis of colloidal metal nanocrystals: a comprehensive review on the reductants. Chem Eur J 24:16944–16963. https://doi.org/10.1002/chem.201802194

Schneider CA, Rasband WS, Eliceiri KW (2012) NIH image to ImageJ: 25 years of image analysis. Nat Methods 9:671–675. https://doi.org/10.1038/nmeth.2089

Shen H, Lu G, Zhang T, Liu J, Gu Y, Perriat P, Martini M, Tillement O, Gong Q (2013) Shape effect on a single-nanoparticle-based plasmonic nanosensor. Nanotechnology 24:285502. https://doi.org/10.1088/0957-4484/24/28/285502

Stabryla LM, Johnston KA, Millstone JE, Gilbertson LM (2018) Emerging investigator series: it's not all about the ion: support for particle-specific contributions to silver nanoparticle antimicrobial activity. Environ Sci Nano 5:2047–2068. https://doi.org/10.1039/C8EN00429C

Stamplecoskie K (2015) Silver nanoparticles: from bulk material to colloidal nanoparticles. In: Alarcon EI, Griffith M, Udekwu KI (eds) Silver nanoparticle applications: in the fabrication and design of medical and biosensing devices. Springer International Publishing, Cham, pp 1–12

Tran QH, Nguyen VQ, Le A-T (2013) Silver nanoparticles: synthesis, properties, toxicology, applications and perspectives. Adv Nat Sci Nanosci Nanotechnol 4:033001. https://doi.org/10.1088/2043-6262/4/3/033001

Treichel JL (2004) Antioxidants and ocular cell type differences in cytoprotection from formic acid toxicity in vitro. Toxicol Sci 82:183–192. https://doi.org/10.1093/toxsci/kfh256

Tulve NS, Stefaniak AB, Vance ME, Rogers K, Mwilu S, LeBouf RF, Schwegler-Berry D, Willis R, Thomas TA, Marr LC (2015) Characterization of silver nanoparticles in selected consumer products and its relevance for predicting children's

potential exposures. Int J Hyg Environ Health 218:345–357. https://doi.org/10.1016/j.ijheh.2015.02.002

Yang T-H, Gilroy DK, Xia Y (2017) Reduction rate as a quantitative knob for achieving deterministic synthesis of colloidal metal nanocrystals. Chem Sci 8:6730–6749. https://doi.org/10.1039/C7SC02833D

Zook JM, Long SE, Cleveland D, Geronimo CLA, MacCuspie RI (2011) Measuring silver nanoparticle dissolution in complex biological and environmental matrices using UV–visible absorbance. Anal Bioanal Chem 401:1993–2002. https://doi.org/10.1007/s00216-011-5266-y

Publisher's note Springer Nature remains neutral with regard to jurisdictional claims in published maps and institutional affiliations.